JACS
JOURNAL OF THE AMERICAN CHEMICAL SOCIETY

Article

pubs.acs.org/JACS

Site-Selective Nucleation and Size Control of Gold Nanoparticle Photothermal Antennae on the Pore Structures of a Virus

Candace E. Benjamin,[†] Zhuo Chen,[†] Peiyuan Kang,[§] Blake A. Wilson,[†] Na Li,[†] Steven O. Nielsen,[†] Zhenpeng Qin,*[,‡,§,∥] and Jeremiah J. Gassensmith*[,†,‡]

[†]Department of Chemistry and Biochemistry, [‡]Department of Biomedical Engineering, [§]Department of Mechanical Engineering, The University of Texas at Dallas 800 West Campbell Road, Richardson, Texas 75080-3021, United States

[∥]Department of Surgery, The University of Texas Southwestern Medical Center, 5323 Harry Hines Blvd., Dallas, Texas 75390, United States

Supporting Information

ABSTRACT: In this Article, we show that the surface of the bacteriophage Qβ is equipped with natural ligands for the synthesis of small gold nanoparticles (AuNP). By exploiting disulfides in the protein secondary structure and the geometry formed from the capsid quaternary structure, we find that we can produce regularly arrayed patterns of ~6 nm AuNPs across the surface of the virus-like particle. Experimental and computational analyses provide insight into the formation and stability of this composite. We further show that the entrapped genetic material can hold upward of 500 molecules of the anticancer drug Doxorubicin without leaking and without interfering with the synthesis of the AuNPs. This direct nucleation of nanoparticles on the capsid allows for exceptional conduction of photothermal energy upon nanosecond laser irradiation. As a proof of principle, we demonstrate that this energy is capable of rapidly releasing the drug from the capsid without heating the bulk solution, allowing for highly targeted cell killing in vitro.

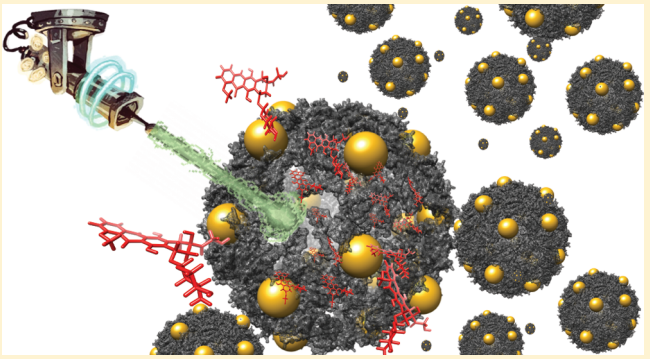

INTRODUCTION

The explosive growth in the synthesis of inorganic materials, specifically plasmonic gold nanoparticles (AuNPs) with controlled nanostructures, has led to several divergent applications in the biomedical and materials fields.[1−7] Among the possible strategies to create homogeneously sized AuNPs, biomolecular templates such as proteins,[8] nucleic acids,[9−11] biological fibers,[12] and lipids[13,14] have emerged, because of the ordered and well-defined structures that these macromolecules form. In addition to these structural advantages, the utilization of biotemplates can impart additional characteristics to these nanomaterials, including solution stability, three-dimensional architectures, molecular and cellular recognition, and tunability for optimized cell uptake.[15−19] These emergent characteristics permit advanced applications such as concomitant drug delivery and in vivo imaging.

Virus-like particles (VLPs),[20] which are the noninfectious[21,22] proteinaceous nanoparticle analogues of viruses, are proven templates[23−26] for the synthesis of metal nanoparticles, because they are innately monodisperse in size and can be genetically modified[27,28] or chemically functionalized[29−31] to attach stabilizing ligands or residues onto their surface with atomistic precision. While there have been several instructive reports on coating,[32] absorbing,[33−42] or growing large AuNPs[5,23,24,42−48] onto or within viral capsids using surface-exposed residues, reports on restricting the diameter of the nanoparticles by constraining their growth to a homogeneous sub-7 nm size have not been forthcoming. This is an important issue because nanoparticle size is critically linked to clearance from blood and tissues,[49−52] and cell-specific uptake and distribution has been linked to nanoparticle diameter.[53] To address this problem, we seek to utilize a multivalent strategy to decorate a proteinaceous biocompatible VLP[54] with multiple small plasmonic AuNPs. From here, these small clustered AuNPs could serve as X-ray or positron emission tomography (PET) contrast agents.[55] We are particularly interested in their use as photothermal antennae as a way to convert pulsed optical radiation to a potent yet extremely localized external stimulus to activate drug release. Indeed, the growth of AuNPs directly onto the protein surface should increase the efficiency of thermal conduction following nanosecond pulsed laser-induced heating. This improved transfer of thermal energy into the protein by direct templated-growth should promote more efficient thermally induced protein denaturation, compared to traditional bioconjugation methods used to attach gold onto protein

Received: September 27, 2018
Published: November 19, 2018

DOI: 10.1021/jacs.8b10446
J. Am. Chem. Soc. XXXX, XXX, XXX−XXX

surfaces via spacers or synthetic ligands.[56] In addition, reports have shown[57,58] that smaller AuNPs possess greater photothermal conversion efficiencies, because of their intrinsically higher absorption/extinction ratios. In principle, templated growth of small AuNPs directly onto a protein surface would mean the amount of gold necessary to induce any changes in protein structure could be reduced, decreasing the likelihood of detectable bioaccumulation even further. Finally, the use of nanosecond pulsed irradiation in this case will confine heating to only a few nanometers of the AuNP, permitting very high thermal-spatial resolution with negligible bulk heating of the solution. In this paper, we report the synthesis and characterization of such a system using VLP Qβ as outlined in Scheme 1. The Qβ capsid itself is an icosahedral virus with 180

Scheme 1. Qβ Possesses 32 Pores, Each Either 1.5 or 3.0 nm in Diameter, Which Are Large Enough To Permit the Diffusion of Doxorubicin into and out of the VLP; after Loading, the Pores Then Are Capped by ~6 nm AuNPs Grown in Situ

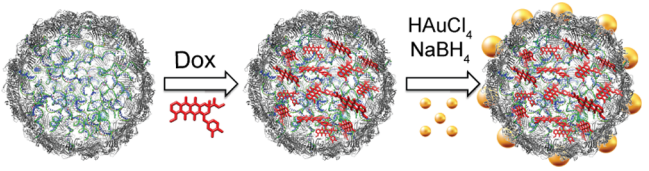

identical coat proteins and contains 32 disulfide-lined pores.[59] We reasoned that these proteins, linked like a daisy chain by either five or six disulfides to form a fixed pore, would act as a natural ligand[60,61] and template for the formation of spherical gold nanoparticles upon in situ reduction of gold salts. We then show that this new composite material works as a proof-of-principle photolytically activated drug delivery vehicle. We can load the capsid with the anticancer drug Doxorubicin (Dox) noncovalently using random RNA located within the capsid as a supramolecular host, grow AuNPs over the loaded VLP and, finally, initiate release of the RNA-bound Dox from the center of the virus using nanosecond laser irradiation to disrupt the proteinaceous shell and release the drug molecules from the interior. Finally, we demonstrate highly selective drug release and cell killing of macrophage and cancer cells in vitro exclusively within the laser path while cells outside the path—even though they are in the same culture—show no drug release or death.

RESULTS AND DISCUSSION

Synthesis and Characterization of AuNP@Qβ. The Qβ VLP, structurally depicted in Figure 1, is expressed as a noninfectious nanoparticle that self-assembles around random genomic material within *E. coli*. Protein crystallographic analysis reveals 20 pores at the 3-fold axis and 12 smaller pores at the 5-fold axis of symmetry. Key to our strategy is that these pores are lined with solvent-exposed disulfides and we hoped to benefit from the affinity of disulfides toward gold species. To establish an optimized protocol for site-specific growth of AuNPs, parameters including the concentrations of Qβ and tetrachloroauric acid, reaction temperature, and incubation time were individually varied until we had minimized the formation of unstable naked gold particles. After significant optimization, the required conditions for AuNP formation turned out to be quite straightforward—

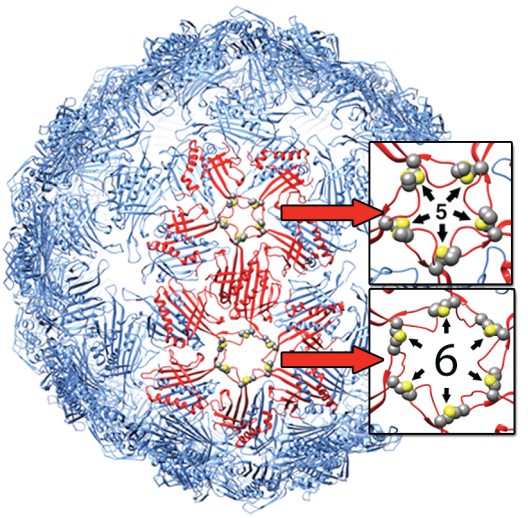

Figure 1. Qβ VLP is depicted as a ribbon model. The VLP has a diameter of 28 nm and contains a total of 32 pores. Depicted are one of the 20 large pores, each of which contains six disulfide bonds, and one of the 12 smaller pores, each of which contains five disulfide bonds.

specific absorption of gold by disulfide bonds was achieved by incubating Qβ and tetrachloroauric acid in water followed by addition of the reducing agent sodium borohydride. Because the water was unbuffered, the final solution was lowered to a pH of 2 by the gold acid; as an alternative, 0.1 M potassium phosphate buffer (pH 7) was used. Once all the reagents were added to the vial, the solution was allowed to stand undisturbed for at least 2 h, during which time its color quickly changed from light red to dark red (Figure S1 in the Supporting Information). Based on ultraviolet−visible light (UV-vis) kinetic analysis following the formation of the surface plasmon, the reaction is 50% complete after 5 min and is >99% complete after 20 min (Figure S2 in the Supporting Information). After the reaction, the small amount of precipitated and unbound AuNPs were removed from the crude mixture by passing the reaction solution through a size-exclusion column. We noted that the nanoparticles in the precipitate increases as we increased the concentration of the acidic gold starting material, which we attribute to a decrease in pH and concomitant protein aggregate formation, which can no longer function as a template.

The selective growth of AuNPs on the pore structures was verified by transmission electron microscopy (TEM) (Figures S3 and S4 in the Supporting Information), which indicated that nearly every VLP contained some population of AuNPs, although it appeared that there was a fairly wide distribution of the number of AuNPs per Qβ. The nanoparticle population dispersity prompted an investigation into the average number of nanoparticles per capsid, which was determined to be ~6 ± 3 per Qβ (Figure S5 in the Supporting Information), as determined by inductively coupled plasma−mass spectroscopy (ICP-MS). Dynamic light scattering (DLS) found an increase in capsid size from 23 nm to 64.83 ± 0.219 nm, which is a significant increase in the size of the capsid (Figure S19 in the Supporting Information). Negative stain was used to show the position of Qβ, relative to the AuNPs. A crystallographic model of Qβ was used to map the AuNPs over the surface. The micrographs shown in Figure 2 exhibit excellent correlation to the mapped pore patterns on the right. This clear association

DOI: 10.1021/jacs.8b10446
J. Am. Chem. Soc. XXXX, XXX, XXX−XXX

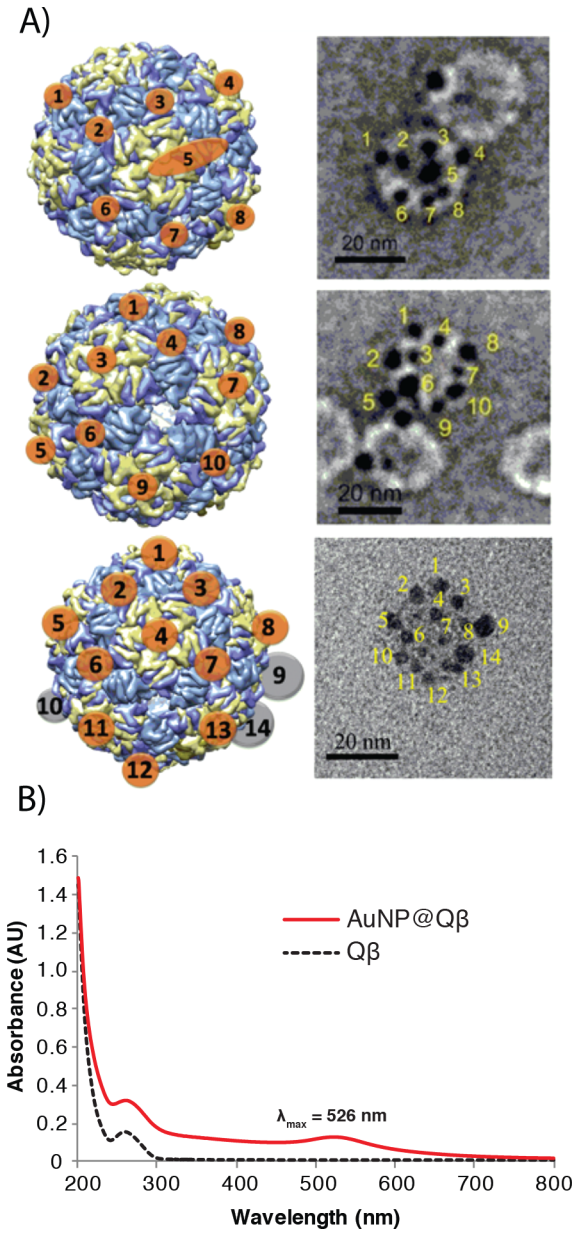

Figure 2. (A) (Left) Illustration of the relative locations of each nanoparticle on Qβ. Orange dots represent AuNPs on pores facing the reader, while gray dots represent AuNPs on pores behind the VLP. (Right) TEM micrograph of AuNP@Qβ synthesized over the pores of Qβ. (B) Ultraviolet−visible light (UV-vis) analysis of Qβ only (black dashed line) and AuNP@Qβ (red line).

of the AuNPs to the pore locations strongly suggests that the pores themselves both selectively nucleate and control the final diameter of the AuNPs. The AuNPs appear fairly monodisperse in size by TEM with a diameter of 3.6 ± 1 nm.

Powder X-ray diffraction (PXRD) confirmed the crystallinity of the as-synthesized AuNPs in the AuNP@Qβ composite, and Rietveld refinement of the data was used to confirm that the bulk as-synthesized diameters of the AuNPs is 6.2 ± 0.2 nm. Regardless, both values are within published cutoff limits for glomerular filtration. In addition, PXRD showed that the structure type of the AuNP is face-centered cubic with the space group *Fm*3*m* (Figure S6 in the Supporting Information). The AuNP@Qβ solution is a deep red color and ultraviolet−visible light (UV-vis) spectra shows an absorption centered at 526 nm, which corresponds to the surface plasmon (Figure 2B). To elucidate the role of the virus in the nucleation and growth of the AuNPs, we conducted several control experiments. When the same procedure was performed in the absence of any Qβ, a dark precipitate formed in solution. This precipitate was collected and was found to consist of spherical AuNPs, as determined by X-ray diffraction and confirmed by transmission electron microscopy (TEM), with a diameter of 48 ± 10 nm (as shown in Figure S6).

To confirm that the disulfides themselves were responsible, we prepared a solution of Qβ and first reduced the disulfides to the free thiols and then alkylated them with 2-iodoacetimide. We obtained the same results as when no Qβ was present in the solution—huge particles in a black precipitate — confirming the role of the disulfides in the controlled nucleation (Figure S1). In our initial strategy, we assumed that reduction of the disulfides was occurring with sodium borohydride, but we were able to rule this out because we did not detect any such reduction using gel electrophoresis (Figure S8 in the Supporting Information) nor was there any appreciable difference in the Ellman's assay before and after the addition of borohydride (Figure S10 in the Supporting Information). It is important to point out that, during the synthesis, even spectroscopically pure virus particles are not fully oxidized—that is to say, it appears from nonreducing sodium dodecyl sulfate−polyacrylamide gel electrophoresis (SDS-PAGE) that monomeric proteins exist when there should be none[62,63] (Figure S9 in the Supporting Information). Curiously, reducing the disulfides to free sulfurs also fails to yield AuNP formation on the surface of the virus. Nevertheless, based on these experiments, it is quite evident that nucleation and size control is occurring as a result of the disulfide and pore geometry, as we get uncontrolled particle growth in their absence.

AuNP@Qβ are stable at room temperature for more than a month when left undisturbed on the bench. TEM micrographs (Figure S11 in the Supporting Information) of a month-old sample that had been left under ambient laboratory conditions show that the AuNPs are still associated with Qβ, and neither free AuNPs nor aggregation was visible. This stability is surprising, considering that (1) the nanoparticles are considerably larger than the pores and (2) there are only 10 or 12 S atoms bound to the nanoparticle. Based on the TEM data, which show varying levels of contrast on the edges of the nanoparticles, we anticipated that there were interactions between the virus and the nanoparticles beyond simply Au−S bonding. Therefore, we conducted computational analysis to determine the likely changes in the local environment around the nanoparticle. As seen in Figure 3, we modeled a 6.4 nm nanoparticle bound to the 12 S atoms of the hexameric pore structure. Molecular dynamics (MD) simulations provide a reasonable picture of the actual nanoparticle−protein interaction. From these simulations, several intriguing results could be inferred (see the expanded discussion of the theory in the Supporting Information and Figures S12−S15; interestingly, there was no significant change in the size of the hexameric pore). However, the pore S atoms shifted radially inward, which created a deeper cavity for the nanoparticle to sit in and, as shown in Figure 3, allowed more of the loop structures present near the pore to cover the surface of the nanoparticle. Roughly 23% of the nanoparticle's surface area was protected by surrounding proteins, which does not significantly change the secondary structure of the VLP, as shown by circular

DOI: 10.1021/jacs.8b10446
J. Am. Chem. Soc. XXXX, XXX, XXX−XXX

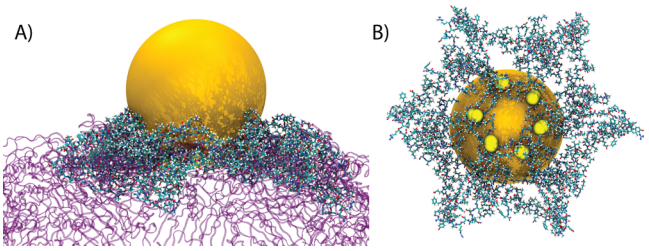

Figure 3. MD simulation snapshots of Qβ with the AuNP at the hexameric pore. (A) Side view of the AuNP and surrounding proteins. The protein segments directly attached to the pore S atoms are shown in a licorice representation, while the rest of the proteins are shown as purple ribbons. (B) A snapshot that shows the pore from below. The pore S atoms are highlighted in yellow. Only the protein segments directly attached to the pore S atoms are shown.

dichroism (CD) measurements (Figure 4D). The stability provided by the surrounding proteins makes sense, because 6-nm naked AuNPs are unstable and subject to rapid Ostwald ripening, resulting in precipitation.[41,42] Being embedded in the virus coat protein not only stabilizes these particles but also protects them—see the Supporting Information for an explanation based on classical nucleation theory and an analysis of the smaller five-membered pores.

Laser-Activated Drug Delivery. AuNPs are well-known photothermal agents and are among the best materials for converting incident optical energy into heat.[44] This heat can be dissipated diffusely into the environment by continuously irradiating the sample, which results in a heating of the bulk solution. Alternatively, heat can be generated very locally by pulsed irradiation, causing the surface of the nanoparticle to heat to several hundred degrees without significantly heating the bulk solution.[45] More than a decade ago, this latter form of pulsed irradiation was found to selectively denature proteins,[46] although, recently, the controlled application of photothermal irradiation to control protein or nucleotide function without damaging the cell has emerged as a potent method of manipulating specific cells in a culture or tissue without affecting the surrounding cells.[56,64] Because the growth of the AuNP occurs directly onto the surface of the protein, we reasoned that, even without 100% gold coverage on each VLP, we would be able to induce a photothermal response using modest laser power. We therefore sought to determine if this mechanism could induce the disruption of the protein shell, triggering the release of entrapped small-molecule drugs. This would enable very localized drug release within a disease microenvironment without damaging nearby healthy cells.

To do this, we exploited the fact that random *E. coli* nucleotides serve as templates in the self-assembly of recombinant Qβ coat proteins to form the intact capsid. Consequently, random bacterial RNA becomes entrapped within the fully assembled VLP. We hypothesized that this genetic material could be used as a supramolecular host capable of noncovalently trapping the strong nucleotide intercalator Doxorubicin (Dox), which is a fluorescent chemotherapeutic that is used in many different cancer therapies. Binding of Dox to VLP RNA is not without precedent, as researchers have shown[47] that the RNA inside the red clover necrotic mosaic virus capsid tightly holds upward of 4300 molecules of Dox. Our tests show that the genetic material inside Qβ does the same: when Dox is bound inside the VLP, the fluorescence is modestly quenched (Figures 4A–C and Figure S16 in the Supporting Information), and when it is released—following boiling of the capsid

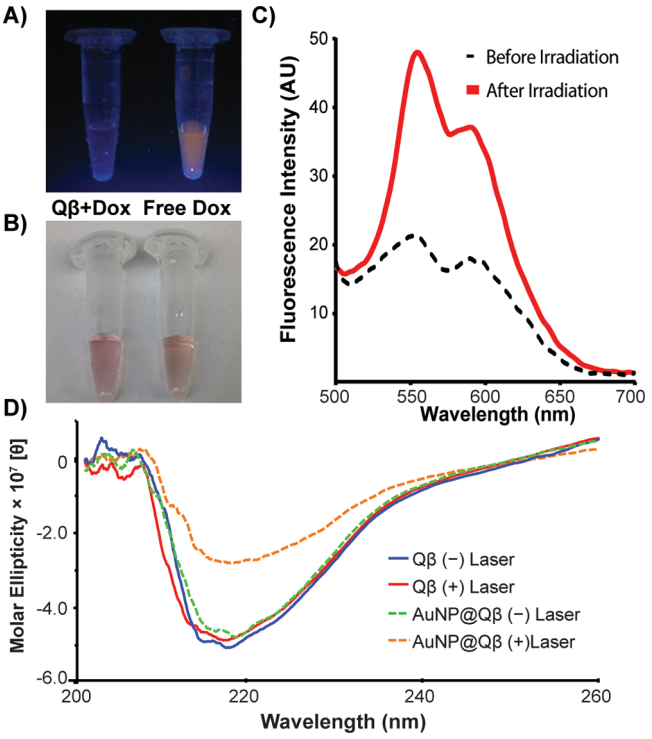

Figure 4. (A) Photographs of Qβ(Dox) prior to irradiation and free Dox under 365 nm UV-light. The fluorescence is quenched in the left vial, as a result of its interaction with the genetic material entrapped in the VLP. (B) Photographs of the same vials shown in panel A under white light. (C) Fluorescence traces of AuNP@Qβ(Dox) before (black dashed line) and after (red solid line) irradiation. (D) CD spectra of Qβ and AuNPs@Qβ before (−) and after (+) laser radiation, showing reduction of CD signal after laser irradiation.

in water, for instance —it fluoresces. The association of Dox to the nucleic acids inside the Qβ is sufficiently high that, after loading, we observe no leakage, even after 24 h (Figure S17 in the Supporting Information). Thus, we can monitor the release by following any fluorescence enhancement after laser irradiation.

To create the Dox-loaded, gold-bespeckled, viral nanoparticles, we followed a procedure outlined in Scheme 1. Initially, the Qβ is loaded by incubating the VLP in a 1 mg/mL solution of Dox for 10 min at room temperature. This mixture is then filtered through a cross-linked dextran size-exclusion column to remove unbound Dox to create Qβ(Dox) (Figure S18 in the Supporting Information). The filtered solution of Qβ(Dox) was then subjected to the same procedure to grow AuNPs over the surface. This solution was again passed through a size-exclusion column to remove unattached nanoparticles and excess salts to yield pure AuNP@Qβ(Dox). By TEM, we saw no discernible difference in gold loading over the pores nor any changes in nanoparticle sizes. We were pleased to see that we could load upward of 500 molecules of Dox—as determined by UV-vis spectroscopy—without interfering with the AuNP formation on the shell.

A 70 μL solution at a concentration of 0.04 mg/mL AuNP@Qβ(Dox) was then irradiated with a single 6-ns laser pulse at an energy density of 500 mJ/cm^2 and centered at a wavelength of 532 nm. The solution temperature was monitored using a

DOI: 10.1021/jacs.8b10446
J. Am. Chem. Soc. XXXX, XXX, XXX−XXX

thermocouple and no bulk solution temperature change was observed. Based on fluorescence analysis of the irradiated sample, a 100% enhancement in fluorescence was seen, indicating that Dox was released from the capsid. Under control conditions, with no laser irradiation, no fluorescence change was observed because the Dox is tightly bound to the RNA (Figures 4A–C). In a second control, which uses convective heat, we found we could replicate these results by boiling AuNP@Qβ(Dox) in water for 5 min, which completely denatured and destroyed the viral capsule. At room temperature, however, the AuNP@Qβ(Dox) was stable for several hours and showed little variation in fluorescence. We conducted CD and DLS spectroscopic studies (Figure 4D and Figure S19 in the Supporting Information) to determine if the photothermal energy was transferred to the protein. Specifically, we looked at samples of Qβ VLP with and without AuNPs to determine if any obvious change in the spectra of theses samples could be ascertained. When AuNP@Qβ was irradiated, a decrease and slight shift in molar ellipticity could be seen, indicating changes in secondary structure and in nanoparticle absorbance (Figure 4D), suggesting some precipitation of aggregates. Agarose band shift assays (Figure S21 in the Supporting Information) showed clear Dox release by UV imaging and a loss or change in capsid structure, following irradiation. In a control experiment using laser irradiation centered at 1064 nm, no change was evident by DLS or agarose band shift (Figures S19 and S21). We therefore attribute this heat to localized absorption of the laser light to generate thermal energy via localized surface plasmon resonance (LSPR), which, in turn, denatures the capsid proteins and provides sufficient thermal energy to release the Dox. This localized heat denaturation and drug release causes a slight shift in the nanoparticle absorbance (Figure S20 in the Supporting Information), denaturation of the protein capsid, and release of the drug, as shown by bandshift assays (Figure S21) in agarose gel electrophoresis.

In order to move toward studies in cellular systems, we first had to determine the toxicity of our particles via MTT assay, using each of the Qβ constructs without the use of laser activation (Figure 5A). The assay found no significant cell viability difference when Qβ(Dox), AuNP@Qβ, and AuNP@Qβ(Dox) were incubated with RAW 264.7 cells. On the other hand, the cells clearly responded to free Dox. A key advantage of this extreme confinement of thermal energy is that it should enable a highly targeted release of therapeutics exclusively within the path of a focused beam of light. In other words, we should be able to pinpoint the cells we wish to kill in a single culture without affecting the surrounding cells, because of convective heat loss. To demonstrate the efficacy of our approach in vitro, cell studies were performed using RAW 264.7 macrophage and A549 lung cancer cells. For the macrophage cells, 3-cm glass bottom plates were seeded with ~1 × 10^6 cells 1–2 days prior to the experiment producing cells that reached ~80% confluency. The cells were then incubated with 240 μL of 0.2 mg/mL AuNP@Qβ(Dox)—equivalent to ~7.8 μM Dox, as well as appropriate controls for 4 h. The cells were washed three times with PBS, stained with 200 nm Hoechst 34442 and washed again with PBS. The plates were covered with a cardboard mask pierced with an 18-gauge needle to confine the laser path to a diameter of 1.27 mm to demonstrate the spatial selectivity of release. The cells were then subject to a single 6-ns pulse of 500 mJ/cm^2 and immediately imaged by live-cell fluorescence microscopy.

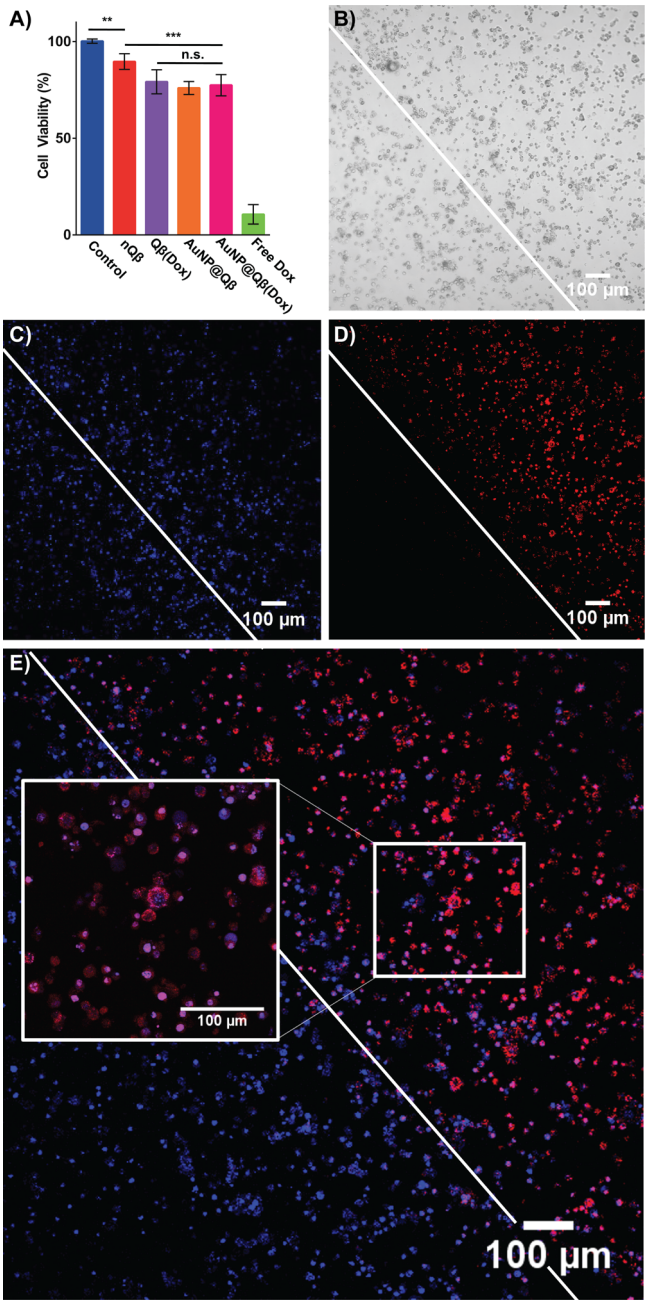

Figure 5. (A) MTT assay of cells treated with Qβ composites or free Dox and incubated to monitor cell viability after 4 h. Double asterisk symbol (**) and triple asterisk symbol (***) denote *P* values of ≤0.01 and 0.001, respectively. (B–D) Wide-field live cell images depicting Dox release after laser irradiation through a pinhole (white line indicates the perimeter of laser irradiation): (B) bright-field image, (C) blue channel showing Hoechst 34442 nuclear dye, and (D) Dox. (E) Merged images acquired with a 10× objective focused near the center of the plate immediately following laser exposure. Cells located close to the aperture experience the release of Dox into the cellular space while those further away do not exhibit the same release.

Immediately following laser irradiation, the release of Dox in the targeted "kill-zone" to the right of the white line in Figures 5B–E was obvious in the red channel of our fluorescence microscope. The morphology of the cells, as shown in Figure 5E and at higher magnification (inset), did not immediately change following irradiation, indicating that the initial laser

DOI: 10.1021/jacs.8b10446
J. Am. Chem. Soc. XXXX, XXX, XXX–XXX

itself did not affect the cells (also shown in Figure S22 in the Supporting Information). However, fluorescence imaging revealed extensive Dox release in the kill zone with the correlation between cells showing release and those within the targeted area being very high; outside of this area, no red fluorescence could be discerned. The highly targeted nature of laser irradiation makes bulk cell viability assays such as MTT ineffective; therefore, we monitored cell viability via live-cell fluorescence imaging for 12 h. Cells outside the kill zone remained intact and adherent, and their morphology was generally unchanged. Within the kill zone, the resulting cells largely detached from the plate after 12 h (Figure S23 in the Supporting Information), indicating that they were killed. When the experiment was repeated using 1064 nm laser light, which is incapable of exciting the LSPR, the results of live cell imaging clearly show no DOX release and no toxicity over that same 12 h time period (Figure S24 in the Supporting Information), again demonstrating that the release is attributed to highly localized optical excitation of the proteinaceous gold complex within the living cell. We repeated these experiments on A549 cells and obtained similar results. In the case of A549 cells, we confirmed cell death exclusively in the laser path using NucRed Dead 647 after allowing the cells to incubate for 4 h (Figure S25 in the Supporting Information). Taken together, these results show that we can release a supramolecularly bound chemotherapeutic from random RNA using photothermally triggered degradation of a protein complex for highly localized cell killing.

CONCLUSION

Using the strong affinity between disulfides and gold species, we have shown that AuNPs can be synthesized site-selectively in a controlled manner on the pore structures of Qβ through a simple incubation and reducing process. TEM micrographs show a well-ordered topology of AuNP@Qβ in accordance with the pattern of pores on Qβ. The growth of the nanoparticles is clearly dependent upon the existence of disulfides as reduction to free sulfurs or acylation of these sulfurs fails to yield the composite material. The resulting AuNP@Qβ is stable, when left exposed on the benchtop at room temperature for more than one month, even though the AuNPs themselves are prone to self-aggregation. Computational modeling indicates this stability arises from surface passivation by local protein physisorption. We found that the growth of AuNPs on the VLP is unaffected by loading the interior with the anticancer drug Doxorubicin. We successfully demonstrated that this new AuNP@Qβ(Dox) composite can release the Dox upon nanosecond-pulsed irradiation without heating the bulk solution and thus offers a pathway to drug delivery with very high spatial resolution. This proof-of-concept shows great promise in using laser irradiation to trigger the release of materials confined within proteinaceous capsids and adds another tool in the arsenal of photothermally activated nanotherapeutics.

ASSOCIATED CONTENT

Supporting Information

The Supporting Information is available free of charge on the ACS Publications website at DOI: 10.1021/jacs.8b10446.

Detailed experimental and synthetic procedures as well as the characterization of the materials presented in this work (PDF)

AUTHOR INFORMATION

Corresponding Authors

*E-mail: zhenpeng.qin@utdallas.edu (Z. Qin).
*E-mail: gassensmith@utdallas.edu (J. J. Gassensmith).

ORCID

Candace E. Benjamin: 0000-0002-9211-718X
Zhuo Chen: 0000-0001-7775-7579
Steven O. Nielsen: 0000-0003-3390-3313
Zhenpeng Qin: 0000-0003-3406-3045
Jeremiah J. Gassensmith: 0000-0001-6400-8106

Author Contributions

The manuscript was written through contributions of all authors. All authors have given approval to the final version of the manuscript.

Funding

C.E.B. thanks the National Science Foundation Graduate Research Fellows Program (No. 1746053) for their support. J.J.G. acknowledges the National Science Foundation (No. DMR-1654405) and the Cancer Prevention and Research Institute of Texas (CPRIT) (No. RP170752). Z.Q. acknowledges support from the National Science Foundation (No. 1631910) and CPRIT (No. RP160770).

Notes

The authors declare no competing financial interest.

ACKNOWLEDGMENTS

We thank Professor M. G. Finn and his student Jenny for their helpful advice, guidance, and generous donation of the Qβ plasmid.

ABBREVIATIONS

VLP, virus-like particle; Dox, Doxorubicin; AuNP, gold nanoparticle; CD, circular dichroism; MD, molecular dynamics; TEM, transmission electron microscopy; PXRD, powder X-ray diffraction; EPR, enhanced permeability and retention

REFERENCES

(1) Mao, C.; Solis, D. J.; Reiss, B. D.; Kottmann, S. T.; Sweeney, R. Y.; Hayhurst, A.; Georgiou, G.; Iverson, B.; Belcher, A. M. Virus-Based Toolkit for the Directed Synthesis of Magnetic and Semiconducting Nanowires. *Science* **2004**, *303* (5655), 213−217.

(2) Bromley, K. M.; Patil, A. J.; Perriman, A. W.; Stubbs, G.; Mann, S. Preparation of high quality nanowires by tobacco mosaic virus templating of gold nanoparticles. *J. Mater. Chem.* **2008**, *18* (40), 4796−4801.

(3) Fernandes, R.; Li, M.; Dujardin, E.; Mann, S.; Kanaras, A. G. Ligand-mediated self-assembly of polymer-enveloped gold nanoparticle chains and networks. *Chem. Commun.* **2010**, *46* (40), 7602−7604.

(4) Mann, S. Self-assembly and transformation of hybrid nano-objects and nanostructures under equilibrium and non-equilibrium conditions. *Nat. Mater.* **2009**, *8* (10), 781−792.

(5) Zhou, K.; Zhang, J.; Wang, Q. Site-Selective Nucleation and Controlled Growth of Gold Nanostructures in Tobacco Mosaic Virus Nanotubulars. *Small* **2015**, *11* (21), 2505−2509.

(6) Shenton, W.; Davis, S. A.; Mann, S. Directed Self-Assembly of Nanoparticles into Macroscopic Materials Using Antibody−Antigen Recognition. *Adv. Mater.* **1999**, *11* (6), 449−452.

(7) Li, F.; Wang, Q. Fabrication of Nanoarchitectures Templated by Virus-Based Nanoparticles: Strategies and Applications. *Small* **2014**, *10* (2), 230−245.

DOI: 10.1021/jacs.8b10446
J. Am. Chem. Soc. XXXX, XXX, XXX−XXX

(8) Xie, J.; Zheng, Y.; Ying, J. Y. Protein-Directed Synthesis of Highly Fluorescent Gold Nanoclusters. *J. Am. Chem. Soc.* **2009**, *131* (3), 888−889.
(9) Lim, D.-K.; Jeon, K.-S.; Hwang, J.-H.; Kim, H.; Kwon, S.; Suh, Y. D.; Nam, J.-M. Highly uniform and reproducible surface-enhanced Raman scattering from DNA-tailorable nanoparticles with 1-nm interior gap. *Nat. Nanotechnol.* **2011**, *6* (7), 452−460.
(10) Samson, J.; Piscopo, I.; Yampolski, A.; Nahirney, P.; Parpas, A.; Aggarwal, A.; Saleh, R.; Drain, C. M., Fabrication of Size-Tunable Metallic Nanoparticles Using Plasmid DNA as a Biomolecular Reactor. *Nanomaterials* **2011**, *1* (1).6478
(11) Raeesi, V.; Chou, L. Y. T.; Chan, W. C. W. Tuning the Drug Loading and Release of DNA-Assembled Gold-Nanorod Superstructures. *Adv. Mater.* **2016**, *28* (38), 8511−8518.
(12) Scheibel, T.; Parthasarathy, R.; Sawicki, G.; Lin, X.-M.; Jaeger, H.; Lindquist, S. L. Conducting nanowires built by controlled self-assembly of amyloid fibers and selective metal deposition. *Proc. Natl. Acad. Sci. U. S. A.* **2003**, *100* (8), 4527−4532.
(13) Patil, A. J.; Muthusamy, E.; Seddon, A. M.; Mann, S. Higher-Order Synthesis of Organoclay Pipes Using Self-Assembled Lipid Templates. *Adv. Mater.* **2003**, *15* (21), 1816−1819.
(14) Burkett, S. L.; Mann, S. Spatial organization and patterning of gold nanoparticles on self-assembled biolipid tubular templates. *Chem. Commun.* **1996**, No. 3, 321−322.
(15) Crookes-Goodson, W. J.; Slocik, J. M.; Naik, R. R. Bio-directed synthesis and assembly of nanomaterials. *Chem. Soc. Rev.* **2008**, *37* (11), 2403−2412.
(16) Li, L.; Liu, J.; Yang, X.; Huang, J.; He, D.; Guo, X.; Wan, L.; He, X.; Wang, K. Biomimetic synthesis of highly biocompatible gold nanoparticles with amino acid-dithiocarbamate as a precursor for SERS imaging. *Nanotechnology* **2016**, *27* (10), 105603.
(17) Gazit, E. Use of biomolecular templates for the fabrication of metal nanowires. *FEBS J.* **2007**, *274* (2), 317−322.
(18) Huang, J.; Lin, L.; Sun, D.; Chen, H.; Yang, D.; Li, Q. Bio-inspired synthesis of metal nanomaterials and applications. *Chem. Soc. Rev.* **2015**, *44* (17), 6330−6374.
(19) de la Escosura, A.; Nolte, R. J. M.; Cornelissen, J. J. L. M. Viruses and protein cages as nanocontainers and nanoreactors. *J. Mater. Chem.* **2009**, *19* (16), 2274−2278.
(20) Chen, Z.; Li, N.; Li, S.; Dharmarwardana, M.; Schlimme, A.; Gassensmith, J. J. Viral chemistry: the chemical functionalization of viral architectures to create new technology. *Wiley Interdiscip. Rev.: Nanomed. Nanobiotechnol.* **2016**, *8*, 512−534.
(21) Akahata, W.; Yang, Z.-Y.; Andersen, H.; Sun, S.; Holdaway, H. A.; Kong, W.-P.; Lewis, M. G.; Higgs, S.; Rossmann, M. G.; Rao, S.; Nabel, G. J. A virus-like particle vaccine for epidemic Chikungunya virus protects nonhuman primates against infection. *Nat. Med.* **2010**, *16* (3), 334−338.
(22) Naskalska, A.; Pyrc, K. Virus like particles as immunogens and universal nanocarriers. *Pol. J. Microbiol.* **2015**, *64* (1), 3−13.
(23) Slocik, J. M.; Naik, R. R.; Stone, M. O.; Wright, D. W. Viral templates for gold nanoparticle synthesis. *J. Mater. Chem.* **2005**, *15* (7), 749−753.
(24) Zhou, Z.; Bedwell, G. J.; Li, R.; Bao, N.; Prevelige, P. E.; Gupta, A. P22 virus-like particles constructed Au/CdS plasmonic photocatalytic nanostructures for enhanced photoactivity. *Chem. Commun.* **2015**, *51* (6), 1062−1065.
(25) Aljabali, A. A. A.; Barclay, J. E.; Lomonossoff, G. P.; Evans, D. J. Virus templated metallic nanoparticles. *Nanoscale* **2010**, *2* (12), 2596−2600.
(26) de la Escosura, A.; Verwegen, M.; Sikkema, F. D.; Comellas-Aragonès, M.; Kirilyuk, A.; Rasing, T.; Nolte, R. J. M.; Cornelissen, J. J. L. M. Viral capsids as templates for the production of monodisperse Prussian blue nanoparticles. *Chem. Commun.* **2008**, No. 13, 1542−1544.
(27) Fiedler, J. D.; Higginson, C.; Hovlid, M. L.; Kislukhin, A. A.; Castillejos, A.; Manzenrieder, F.; Campbell, M. G.; Voss, N. R.; Potter, C. S.; Carragher, B.; Finn, M. G. Engineered Mutations Change the Structure and Stability of a Virus-Like Particle. *Biomacromolecules* **2012**, *13* (8), 2339−2348.
(28) Brown, S. D.; Fiedler, J. D.; Finn, M. G. Assembly of Hybrid Bacteriophage Qβ Virus-like Particles. *Biochemistry* **2009**, *48* (47), 11155−11157.
(29) Yin, Z.; Comellas-Aragones, M.; Chowdhury, S.; Bentley, P.; Kaczanowska, K.; BenMohamed, L.; Gildersleeve, J. C.; Finn, M. G.; Huang, X. Boosting Immunity to Small Tumor-Associated Carbohydrates with Bacteriophage Qβ Capsids. *ACS Chem. Biol.* **2013**, *8* (6), 1253−1262.
(30) Pokorski, J. K.; Breitenkamp, K.; Liepold, L. O.; Qazi, S.; Finn, M. G. Functional Virus-Based Polymer−Protein Nanoparticles by Atom Transfer Radical Polymerization. *J. Am. Chem. Soc.* **2011**, *133* (24), 9242−9245.
(31) Strable, E.; Finn, M. G. Chemical modification of viruses and virus-like particles. In *Viruses and Nanotechnology*; Manchester, M., Steinmetz, N. F., Eds.; Current Topics in Microbiology and Immunology, Vol. *327*; Springer: Berlin, Heidelberg, 2009; pp 1−21.
(32) Aljabali, A. A. A.; Lomonossoff, G. P.; Evans, D. J. CPMV-Polyelectrolyte-Templated Gold Nanoparticles. *Biomacromolecules* **2011**, *12* (7), 2723−2728.
(33) Huang, Y.; Chiang, C.-Y.; Lee, S. K.; Gao, Y.; Hu, E. L.; Yoreo, J. D.; Belcher, A. M. Programmable Assembly of Nanoarchitectures Using Genetically Engineered Viruses. *Nano Lett.* **2005**, *5* (7), 1429−1434.
(34) Nagakawa, K.; Niikura, K.; Suzuki, T.; Matsuo, Y.; Igarashi, M.; Sawa, H.; Ijiro, K. Virus Capsid Coating of Gold Nanoparticles via Cysteine−Au Interactions and Their Effective Cellular Uptakes. *Chem. Lett.* **2012**, *41* (1), 113−115.
(35) Blaik, R. A.; Lan, E.; Huang, Y.; Dunn, B. Gold-Coated M13 Bacteriophage as a Template for Glucose Oxidase Biofuel Cells with Direct Electron Transfer. *ACS Nano* **2016**, *10* (1), 324−332.
(36) Li, F.; Chen, H.; Zhang, Y.; Chen, Z.; Zhang, Z.-P.; Zhang, X.-E.; Wang, Q. Three-Dimensional Gold Nanoparticle Clusters with Tunable Cores Templated by a Viral Protein Scaffold. *Small* **2012**, *8* (24), 3832−3838.
(37) Blum, A. S.; Soto, C. M.; Wilson, C. D.; Cole, J. D.; Kim, M.; Gnade, B.; Chatterji, A.; Ochoa, W. F.; Lin, T.; Johnson, J. E.; Ratna, B. R. Cowpea Mosaic Virus as a Scaffold for 3-D Patterning of Gold Nanoparticles. *Nano Lett.* **2004**, *4* (5), 867−870.
(38) Li, F.; Chen, H.; Ma, L.; Zhou, K.; Zhang, Z.-P.; Meng, C.; Zhang, X.-E.; Wang, Q. Insights into Stabilization of a Viral Protein Cage in Templating Complex Nanoarchitectures: Roles of Disulfide Bonds. *Small* **2014**, *10* (3), 536−543.
(39) Lee, H.-E.; Lee, H. K.; Chang, H.; Ahn, H.-Y.; Erdene, N.; Lee, H.-Y.; Lee, Y.-S.; Jeong, D. H.; Chung, J.; Nam, K. T. Virus Templated Gold Nanocube Chain for SERS Nanoprobe. *Small* **2014**, *10* (15), 3007−3011.
(40) Zahr, O. K.; Blum, A. S. Solution Phase Gold Nanorings on a Viral Protein Template. *Nano Lett.* **2012**, *12* (2), 629−633.
(41) Blum, A. S.; Soto, C. M.; Sapsford, K. E.; Wilson, C. D.; Moore, M. H.; Ratna, B. R. Molecular electronics based nanosensors on a viral scaffold. *Biosens. Bioelectron.* **2011**, *26* (6), 2852−2857.
(42) Wang, Q.; Lin, T.; Johnson, J. E.; Finn, M. G. Natural Supramolecular Building Blocks. *Chem. Biol.* **2002**, *9* (7), 813−819.
(43) Vera-Robles, L. I.; González-Gracida, J.; Hernández-Gordillo, A.; Campero, A. Using the M13 Phage as a Biotemplate to Create Mesoporous Structures Decorated with Gold and Platinum Nanoparticles. *Langmuir* **2015**, *31* (33), 9188−9197.
(44) Wang, Q.; Lin, T.; Tang, L.; Johnson, J. E.; Finn, M. G. Icosahedral Virus Particles as Addressable Nanoscale Building Blocks. *Angew. Chem.* **2002**, *114* (3), 477−480.
(45) Sun, J.; DuFort, C.; Daniel, M.-C.; Murali, A.; Chen, C.; Gopinath, K.; Stein, B.; De, M.; Rotello, V. M.; Holzenburg, A.; Kao, C. C.; Dragnea, B. Core-controlled polymorphism in virus-like particles. *Proc. Natl. Acad. Sci. U. S. A.* **2007**, *104* (4), 1354−1359.
(46) Tsvetkova, I. B.; Dragnea, B. G., Encapsulation of Nanoparticles in Virus Protein Shells. In *Protein Cages: Methods and Protocols*; Orner, B. P., Ed.; Springer: New York, 2015; pp 1−15.

DOI: 10.1021/jacs.8b10446
J. Am. Chem. Soc. XXXX, XXX, XXX−XXX

(47) Liu, A.; Verwegen, M.; de Ruiter, M. V.; Maassen, S. J.; Traulsen, C. H. H.; Cornelissen, J. J. L. M. Protein Cages as Containers for Gold Nanoparticles. *J. Phys. Chem. B* **2016**, *120* (26), 6352−6357.
(48) Liu, A.; Traulsen, C. H. H.; Cornelissen, J. J. L. M. Nitroarene Reduction by a Virus Protein Cage Based Nanoreactor. *ACS Catal.* **2016**, *6* (5), 3084−3091.
(49) De Jong, W. H.; Hagens, W. I.; Krystek, P.; Burger, M. C.; Sips, A. J. A. M.; Geertsma, R. E. Particle size-dependent organ distribution of gold nanoparticles after intravenous administration. *Biomaterials* **2008**, *29* (12), 1912−1919.
(50) Chou, L. Y. T.; Zagorovsky, K.; Chan, W. C. W. DNA assembly of nanoparticle superstructures for controlled biological delivery and elimination. *Nat. Nanotechnol.* **2014**, *9* (2), 148−155.
(51) Longmire, M.; Choyke, P. L.; Kobayashi, H. Clearance properties of nano-sized particles and molecules as imaging agents: considerations and caveats. *Nanomedicine* **2008**, *3* (5), 703−717.
(52) Blanco, E.; Shen, H.; Ferrari, M. Principles of nanoparticle design for overcoming biological barriers to drug delivery. *Nat. Biotechnol.* **2015**, *33* (9), 941−951.
(53) Shang, L.; Nienhaus, K.; Nienhaus, G. U. Engineered nanoparticles interacting with cells: size matters. *J. Nanobiotechnol.* **2014**, *12* (1), 5.
(54) Singh, P.; Prasuhn, D.; Yeh, R. M.; Destito, G.; Rae, C. S.; Osborn, K.; Finn, M. G.; Manchester, M. Bio-distribution, toxicity and pathology of cowpea mosaic virus nanoparticles in vivo. *J. Controlled Release* **2007**, *120* (1−2), 41−50.
(55) Zhou, C.; Hao, G.; Thomas, P.; Liu, J.; Yu, M.; Sun, S.; Öz, O. K.; Sun, X.; Zheng, J. Near-Infrared Emitting Radioactive Gold Nanoparticles with Molecular Pharmacokinetics. *Angew. Chem.* **2012**, *124* (40), 10265−10269.
(56) Kang, P.; Chen, Z.; Nielsen, S. O.; Hoyt, K.; D'Arcy, S.; Gassensmith, J. J.; Qin, Z. Molecular Hyperthermia: Spatiotemporal Protein Unfolding and Inactivation by Nanosecond Plasmonic Heating. *Small* **2017**, *13* (36), 1700841.
(57) Jiang, K.; Smith, D. A.; Pinchuk, A. Size-Dependent Photothermal Conversion Efficiencies of Plasmonically Heated Gold Nanoparticles. *J. Phys. Chem. C* **2013**, *117* (51), 27073−27080.
(58) Chen, H.; Shao, L.; Ming, T.; Sun, Z.; Zhao, C.; Yang, B.; Wang, J. Understanding the Photothermal Conversion Efficiency of Gold Nanocrystals. *Small* **2010**, *6* (20), 2272−2280.
(59) Golmohammadi, R.; Fridborg, K.; Bundule, M.; Valegård, K.; Liljas, L. The crystal structure of bacteriophage Qβ at 3.5 å resolution. *Structure* **1996**, *4* (5), 543−554.
(60) Letsinger, R. L.; Elghanian, R.; Viswanadham, G.; Mirkin, C. A. Use of a Steroid Cyclic Disulfide Anchor in Constructing Gold Nanoparticle−Oligonucleotide Conjugates. *Bioconjugate Chem.* **2000**, *11* (2), 289−291.
(61) Hakkinen, H. The gold-sulfur interface at the nanoscale. *Nat. Chem.* **2012**, *4* (6), 443−455.
(62) Chen, Z.; Boyd, S. D.; Calvo, J. S.; Murray, K. W.; Mejia, G. L.; Benjamin, C. E.; Welch, R. P.; Winkler, D. D.; Meloni, G.; D'Arcy, S.; Gassensmith, J. J. Fluorescent Functionalization across Quaternary Structure in a Virus-like Particle. *Bioconjugate Chem.* **2017**, *28* (9), 2277−2283.
(63) Chen, Z.; Li, N.; Chen, L.; Lee, J.; Gassensmith, J. J. Dual Functionalized Bacteriophage Qβ as a Photocaged Drug Carrier. *Small* **2016**, *12* (33), 4563−4571.
(64) Li, X.; Kang, P.; Chen, Z.; Lal, S.; Zhang, L.; Gassensmith, J. J.; Qin, Z. Rock the nucleus: significantly enhanced nuclear membrane permeability and gene transfection by plasmonic nanobubble induced nanomechanical transduction. *Chem. Commun.* **2018**, *54* (20), 2479−2482.

DOI: 10.1021/jacs.8b10446
J. Am. Chem. Soc. XXXX, XXX, XXX−XXX